ISSN 0036-0295, Russian Metallurgy (Metally), Vol. 2022, No. 5, pp. 520–527. © Pleiades Publishing, Ltd., 2022.
Russian Text © The Author(s), 2022, published in Metally, 2022, No. 3, pp. 65–74.

Effect of the Carbon Content on the Structure and Mechanical Properties of a High-Temperature Carbide-Hardening Niobium–Molybdenum Alloy

I. B. Gnesin[a], *, M. I. Karpov[a], D. V. Prokhorov[a], B. A. Gnesin[a], T. S. Stroganova[a], I. S. Zheltyakova[a], V. I. Vnukov[a], E. I. Ryabenko[a], and I. L. Svetlov[b]

[a] *Institute of Solid State Physics, Russian Academy of Sciences, Chernogolovka, Moscow oblast, Russia*

[b] *All-Russia Research Institute of Aviation Materials, National Scientific Centre Kurchatov Institute, Moscow, Russia*

**e-mail: ibgnesin@issp.ac.ru*

Received December 16, 2021; revised January 19, 2022; accepted February 28, 2022

Abstract—The elemental, phase, and structural state of Nb–Mo–C alloys with equiatomic metal contents and 15, 20, 25, and 30 at % C are studied after electron-beam zone melting. In the alloy containing 15 at %, a fine microstructure, which is typical of eutectic alloys, forms; as the carbon content increases, primary carbide crystals appear in the alloy structure. The main carbide phase in all alloys is found to be an NbC-based carbide rather than an Nb_2C-based carbide. The component distribution between the phases is studied as a function of the average alloy composition. The results of short-time strength tests of alloy specimens at room temperature and at 1500°C and also their high-temperature bending creep tests are presented. The 100-h creep strength maximum for the alloys is shown to be 200–300 MPa at 1500°C (σ_{100}^{1500} = 200–300 MPa).

Keywords: niobium, molybdenum, niobium carbide, strength, creep, phase analysis, microstructure

DOI: 10.1134/S0036029522050044

INTRODUCTION

Searching for high-temperature materials for operating temperatures higher than 1300°C is one of the challenging problems of modern materials science. Niobium-based alloys have a high potential for designing high-temperature structural materials due to their high melting temperature, relatively low density, and quite high fracture toughness at room temperature [1–3]. However, at temperatures higher than 1000°C, the strength of niobium-based alloys significantly decreases [4]; therefore, the balance of such properties of niobium alloys as high-temperature strength, creep, and fracture toughness can be reached only by hardening a niobium matrix. Various methods of hardening are possible: the dissolution of alloying elements (Ti, Al, Zr, V, Mo, Hf, W) in niobium [5–13] or the introduction into a niobium matrix of hardening phases, such as (Nb,Ti)C [14, 15], (Nb,Ti)B [16], (Nb,Zr)C [17], Nb_3Al [18, 19], Nb_3Si, and Nb_5Si_3 [3–6, 20, 21].

Silicide-hardening niobium alloys were studied in [3, 4, 22]. These alloys were shown to withstand loads up to 100–200 MPa at 1200–1300°C for a long time, but these temperatures are likely to be limiting for the alloys. In the structure of the alloys, dislocations were detected near the interface of a niobium matrix and a hardening silicide phase, which demonstrated plastic deformation of both components at during steady-state creep of the composite at 1300°C [3].

The influence of boron on the structure and mechanical properties of composites based on niobium alloys were studied in [16, 23]. Multiphase niobium Nb–Ti–C–B composites containing an Ni-based solid solution ($Nb_{s.s}$) and boride ((Nb,Ti)B) and carbide ((Nb,Ti)C) phases were prepared by arc melting. Phases (Nb,Ti)B), (Nb,Ti)C), and ($Nb_{s.s}$) formed a eutectic network around primary ($Nb_{s.s}$) dendrites. The boride and carbide phases substantially increase the strength and hardness of the composites. A higher boron content favors an increase in the hardness from 304 to 337 *HV*, in the compressive yield strength from 700 to 810 MPa, and the tensile ultimate strength from 535 to 710 MPa but decreases the fracture toughness from 18.6 to 12.7 MPa $m^{1/2}$ [16]. Alloying with tungsten led to a decrease in the primary ($Nb_{s.s}$) dendrite sizes and to coarsening boride (Nb,Ti,W)B precipitates. The test results showed that the hardness and the compressive strength of the composites also increased with the tungsten content. The highest yield strength at 1200°C (241 MPa) was achieved for a composite containing 10 at % W.

Ternary Nb–Zr–C alloys produced by arc melting were studied in [17]. In an alloy with the equiatomic contents of zirconium and carbon, the niobium content was varied from 40 to 90 at %. An increase in the carbide phase content was found to increase the strength of the alloys and to decrease the ductility at low temperatures. The maximum yield strength at 1500°C (300 MPa) was reached for an alloy with 40 at % Nb. An alloy containing 80 at % Nb demonstrated the optimum combination of the compressive strength at 1500°C (~95 MPa) and the fracture toughness at room temperature (~20 MPa $m^{1/2}$).

The authors of [18, 19] showed that the mechanical properties of niobium-based alloys at high temperature effectively increase when an alloy structure simultaneously contains niobium carbide and niobium aluminide. The high-temperature and room-temperature strengths of as-cast and heat-treated (1100°C, 24 h) alloy specimens increased when carbon and aluminum were added, and their ductility decreased due to the formation of a primary brittle carbide. The maximum values $\sigma_{0.2}$ = 383 MPa and σ_u = 424 MPa at 1000°C were reached for an Nb–25Ti–8C–15Al alloy in compression tests.

Eutectic Mo–Nb–$Re_{0.5}$–Ta–W–$(TiC)_x$ composites were developed using thermodynamic calculations and were prepared by arc melting [20]. These composites consisted of a metallic matrix with a bcc structure and multicomponent TiC-based carbide with an fcc structure. When the TiC content in an alloy increases, its microstructure is changed from hypoeutectic to eutectic and, then, hypereutectic. The ultimate strength of the composite increased correspondingly to an increase in the TiC content. The Mo–Nb–$Re_{0.5}$–Ta–W–$(TiC)_x$ composite with a eutectic structure has the highest compression strength (1943 ± 13 MPa) and a yield strength 1496 ± 17 MPa at room temperature. The hardening mechanism was provided by the existence of dispersed carbide particles.

The influence of alloying on the high-temperature creep characteristics of alloys with solid-solution (Nb–Mo–W system) and silicide (Nb–16Si–Mo–W system) hardening at 1500°C was studied in [24]. The creep resistance increased with the molybdenum and tungsten contents in both the ternary alloys and the silicide-hardening alloys. The Nb–16Si–5Mo–15W–5Hf (at %) alloy demonstrates the lowest strain rate. The parameters of the equation describing the process of high-temperature creep, namely, exponent n = 2.4 and activation energy Q = 675 kJ/mol, were calculated for this alloy. Taking into account this value of Q and the available literature data on the activation energies for molybdenum and tungsten in niobium, the authors of [24] supposed that the creep in this alloy is controlled by the diffusion rate of tungsten in the niobium solid solution. Its 100-h compressive creep strength at 1500°C was 180 MPa. This result is record-breaking for silicide-hardening niobium alloys. However, the alloy had a high density and a relatively low fracture toughness, 10 MPa $m^{1/2}$.

Titanium–carbide-hardened borosilicate molybdenum alloys (Mo–Si–B–Ti–C alloys) are also considered as promising high-temperature materials. A detailed description of their structure and mechanical properties in the temperature range 20–1500°C is given in review [25]. The long-term strength of a 65Mo–5Si–10B–10Ti–10C (at %) alloy was studied in [21] during tensile tests in the temperature range 1400–1600°C. The time to fracture of this alloy was 400 h at 1400°C, load 137 MPa, and an exponent n = 3.

The studies performed in [26] showed that the best results for the short-time bending strength at room temperature and at 1500°C and for the creep resistance at 1500°C were obtained on an Nb–Mo–20C (at %) alloy: the short-time bending strength were 330 and 900 MPa, respectively, and the 100-h creep strength in the temperature range 1450–1500°C was 160–190 MPa. These high-temperature properties are record-breaking.

Thus, in spite of the studies carried out over the world, the search for materials characterized by a combination of a high strength and fracture toughness at room temperature and a low high-temperature creep rate with a high strength at a high temperature remains important. The analysis of the available literature data shows the perspective of the approach, which enables one to achieve the best strength characteristics of alloys at high temperatures by hardening high-temperature alloys with carbide phases. Nb–Mo–C alloys have the highest characteristics of high-temperature strength and creep resistance. The main hardening phase in the alloys is a carbide, the composition and structural features of which are determining for the mechanical properties of the material. The purpose of this work is to investigate the influence of the carbon content in Nb–Mo–C alloys on their structure, phase composition, and mechanical properties.

EXPERIMENTAL

We studied specimens of four compositions: $Nb_{42.5}Mo_{42.5}C_{15}$, $Nb_{40}Mo_{40}C_{20}$, $Nb_{37.5}Mo_{37.5}C_{25}$, and $Nb_{35}Mo_{35}C_{30}$ (at %).

The initial materials were a PM99.95 molybdenum powder produced by AO POLEMA, an NbP-3 niobium powder, and N220 carbon black. The powders were carefully mixed and compacted at room temperature (pressure was ~100 MPa). The formed compacts were sintered in vacuum at ~1900°C for 20 min and then remelted on an electron-beam zone melting setup. In melting, a zone passed four times along the specimen length at a speed of 4 mm/min. As a result of zone melting, we prepared ingots 10–14 mm in diameter and 80–100 mm. Specimens for studying the structure and phase composition and for mechanical tests were cut from the ingots on an EDM machine. A

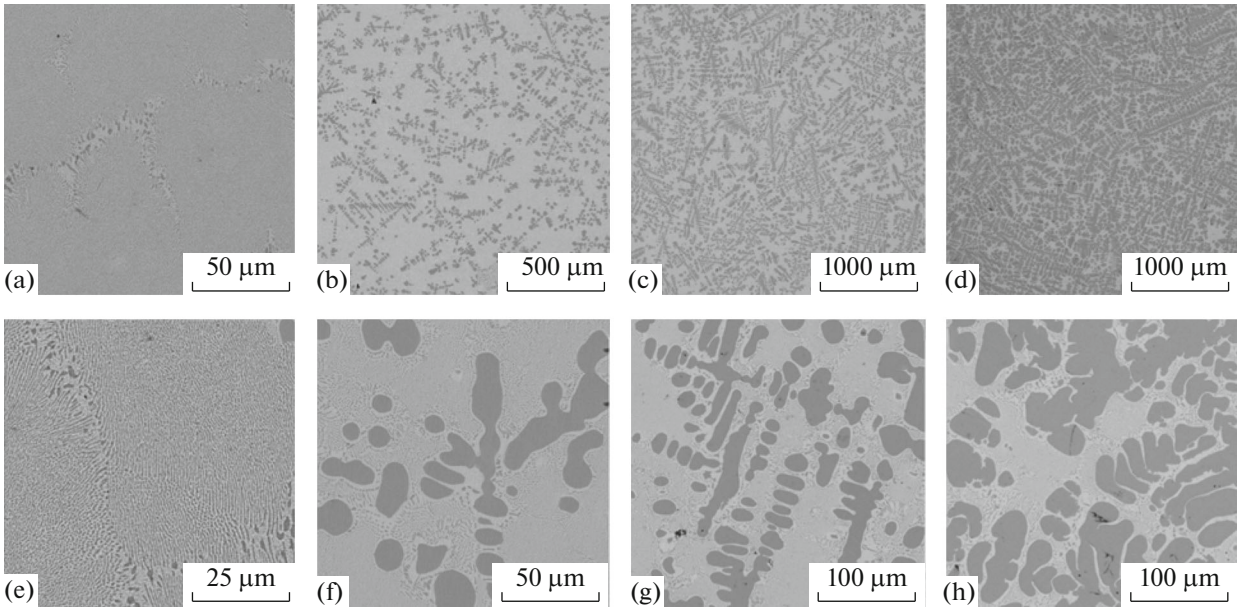

Fig. 1. Microstructure of the cross sections of the ingots of alloys with a carbon content (at %) of (a, e) 15, (b, f) 20, (c, g) 25, and (d, h) 30.

microstructure was studied on the specimens cut perpendicular to the long ingot axis. 2 × 2 × 20-mm specimens for bending strength tests were cut along the long ingot axis. Metallographic sections were prepared using an SiC-based abrasive paper with grain size number up to P2500 and the synthetic diamond powders from ASM 10/7 to ASM 1/0.

The structure and the phase composition of the specimens were analyzed using scanning electron microscopy (SEM; Tescan VEGA-II XMU, CamScan MV230) and X-ray diffraction (XRD; DRON-3M, 20 keV, incident-beam-monochromatized Mo$K\alpha$ radiation). Electron-probe microanalysis (EPMA) was carried out using an INCA Energy 450 energy dispersive spectrometer with a semiconductor Si(Li) INCA X-sight detector. All images of the microstructure of the alloys presented in this work were taken using backscattered electrons.

The volume fractions of the phases were determined by the Glagolev method using microstructure images taken with backscattered electrons [27]. The measurements were carried out using the ImageJ v1.53c program [28]. The fields of view were from 38 × 38 to 152 × 152 μm for a specimen containing 15 at % C and from 152 × 152 to 305 × 305 μm for specimens containing 20–30 at % C. The total number of analysis points on each field of view was 484.

Short-time strength and creep test were carried out at temperatures of 20–1500°C according to the three-point bending scheme in the vacuum chamber of an Instron machine in a high-purity argon atmosphere. To ensure the required rigidity of supports during high-temperature tests, the supports were made of special high-temperature ceramics based on refractory metal carbides.

RESULTS AND DISCUSSION

Structure of Alloys

Figure 1 shows SEM (backscattered electrons) images of the microstructure of the Nb–Mo–C alloys with various carbon contents. All these alloys contained a eutectic two-phase structural component formed by a metallic matrix and a carbide phase. The specimens of the alloys containing 20, 25, and 30 at % C also had primary carbide dendrite crystals.

Thus, the structures of all ternary Nb–Mo–C alloys are represented by a binary metal–carbide eutectic. It should be noted that all alloys have a quite high homogeneity of the distributions of the phases and structural components over the cross section of the specimens. Deviations from the structure characteristic of the main part of a specimen can be observed only at a distance of 500–1000 μm from the external specimen surface (Fig. 2). All SEM and XRD studies were carried out in the central regions of the specimens.

The structure of the alloy with 15 at % C completely consists of eutectic colonies, which are represented by fine mixtures of carbide particles and a metallic matrix. As follows from microstructure images, the carbide particles in the eutectic colonies are likely to have a needle-like shape. It should be noted that the carbide mixture has a quite high dispersion: in all specimens, the characteristic periods of alternating the phases comprising the eutectic were 1 μm,

and individual crystallites in the eutectic colonies have transverse sizes of 200–500 nm.

The main peculiarity of the microstructure of the alloy with 15 at % C is the absence of excess crystals of carbides or a metal-based solid solution, which demonstrates exact correlation between the alloy composition and the binary eutectic point. The regions in the image of the structure of this specimen, within which local coarsening of carbide crystals is observed and the metallic phase is free from carbide particles (Fig. 1a), are eutectic colony junctions. This local change in the structure is most likely to be related to the differences of the solid phase growth conditions in at the final stage of solidification of the remaining small volumes of liquid phase and the existence of solidification centers in the form of existing eutectic colonies, the distance between which at this stage becomes comparable with the characteristic sizes of individual crystallites.

The structure of the alloys with 20, 25, and 30 at % C contained primary carbides (Fig. 1), the volume fraction increased from ~20 to ~60 vol % with the carbon content. It is difficult to exactly estimate the volume fraction of the carbide phase in the eutectic structural component of the alloys due to the high dispersion of carbide particles. Nevertheless, the measured fraction of carbides in the eutectic was ~25 vol % (22–29 vol %) for all alloys. No marked dependence of the carbide fraction in the eutectic on the average alloy composition was observed.

Attention should also be paid to the structural component in the form of the metallic matrix regions bordering primary carbides (Figs. 1f–1h). These regions are free from eutectic carbide precipitates. As follows from the morphology of these regions, the cause of their formation is partial precipitation of eutectic carbide on a primary carbide in the regions adjacent to primary carbides during eutectic solidification. The volume fraction of this structural component (8 to 12 vol %) is obviously to be related to the volume fraction and morphology of the primary carbides in the alloy.

Table 1 gives data on the component distribution over phases for all alloys. Since it is difficult to estimate the carbon content by energy dispersive X-ray spectral analysis reliably and quantitatively, the ratio of signals from metallic components was analyzed for various phases in this work. For this purpose, we introduced parameter R_{Nb}, which is the percentage ratio of the atomic niobium content in a phase to the sum of the atomic niobium and molybdenum contents in this phase.

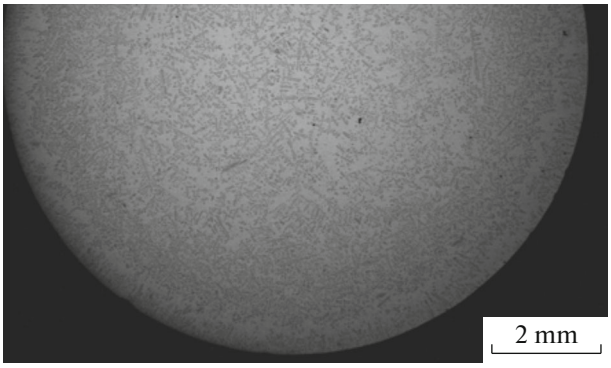

Fig. 2. General appearance of an alloy specimen containing 20 at % C.

The carbide phase in all the alloys was found to be significantly enriched in niobium as compared to the average alloy composition, while the molybdenum content in the metallic phase (solid solution) is higher than that of niobium. The average alloy composition influences the ratio of the molybdenum to niobium contents in the specimens. As the average carbon content in the alloy increases, both phases (carbide and metallic ones) are enriched in molybdenum (Table 1). This phenomenon does not contradict the balance of the components, since one of the phases contains excess niobium (carbide phase), and the other, excess molybdenum (metallic phase). Thus, in spite of an increase in the molybdenum content in both phases, the total balance of the components is retained due to the change in the ratio of their contents in the alloy (increase in the amount of the carbide phase with the average carbon content). For example, in the case of the highest increase in the molybdenum content in the phases (i.e., in the specimen with 30 at % C), the highest volume fraction of the carbide phase, in which a significant excess of niobium is retained, is also detected.

Figure 3 shows the X-ray diffraction patterns of the alloys. According to XRD data, the main phases in all

Table 1. Component distribution over the phases in Nb–Mo–C alloys with various carbon contents

Phase	Value of R_{Nb}, %, in phases of alloy specimens			
	15 at % C	20 at % C	25 at % C	30 at % C
Carbide-based solid solution	89.0	87.0	84.2	83.9
Metal-based solid solution	43.1	33.2	26.2	20.9
Eutectic	53.8	44.3	39.4	35.6

Parameter $R_{Nb} = 100C_{Nb}/(C_{Nb} + C_{Mo})$.

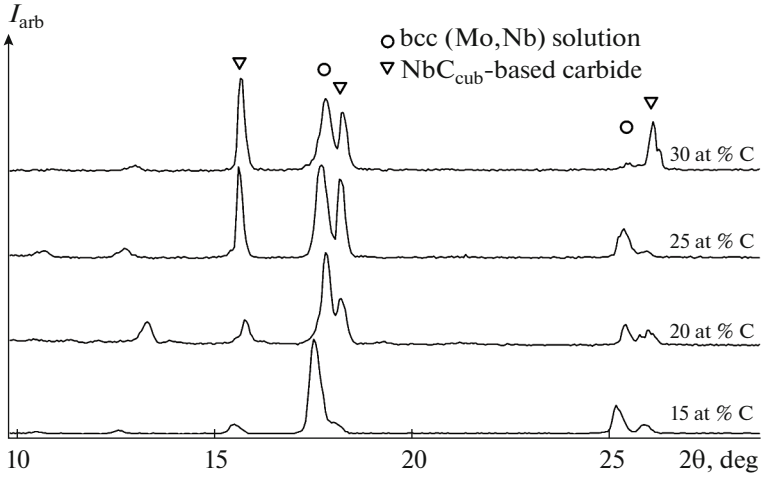

Fig. 3. X-ray diffraction patterns of alloys with various carbon contents.

the specimens are solid solutions: a bcc molybdenum-based (Mo, Nb) solution and a cubic niobium monocarbide-based (NbC_{cub}) solution (Fig. 3). The presence of NbC_{cub}-based rather than Nb_2C-based carbide is relatively unexpected.

The existence of lines in the angular range $2\theta = 10–14$ deg is related to the influence of auxiliary materials, in which specimens were fixed.

The ratio of the line intensities of individual phases in the X-ray diffraction patterns corresponds in many respects to JCDPS powder data; however, there are also deviations from the well-known data (JCDPS PDF nos. 38-1664, 74-5548, 42-1120, 35-0789). This fact demonstrates the existence of a crystallographic texture in the alloys, which can be explained by the well-known peculiarities of solidification during zone melting. However, the general character of changes in the X-ray diffraction patterns of the alloys with increasing carbon content is quite regular. The intensities of the lines corresponding to the metal-based solid solution decrease as the average carbon content in the alloy increases; the reverse situation is characteristic of the carbide lines. This result completely agrees with the data obtained on the volume fractions of the phases in the alloys. In addition, we should also note a general tendency observed in the measured X-ray diffraction patterns to a shift of almost all peaks toward higher angles as the carbon content in the alloy increases. This fact also agrees well with the above data on an increase in the molybdenum contents in both phases as the average carbon content increases. However, it should be remembered that, in the three-component system, the lattice parameter for each phase is determined by both the ratio of the metal contents and the carbon content. Although, as follows from the well-known data (for example, JCPDS 74-5548, 89-2868), the carbon content influences the lattice parameter of the phases more weakly than the ratio of the molybdenum to niobium contents, we cannot eliminate its influence or separate its contribution to the changes in the lattice parameters of the phases at this stage.

We now estimate the presence of cubic niobium monocarbide instead of an Nb_2C-based phase, the formation of which seems to be more likely with allowance for the Mo–C and Nb–C phase diagrams: in these binary systems, the metal-based solid solution is in equilibrium with M_2C rather than MC carbide. We advance the following two hypotheses of the NbC-based phase formation in the alloys:

(i) nucleation as a more refractory phase during primary solidification and conservation in a metastable state due to marked cooling rates during zone melting,

(ii) structural peculiarities of the ternary Nb–Mo–C diagram.

The first hypothesis is thought to be less probable. It is in conflict with the fact that, according to XRD data, the cubic NbC-based phase is the main carbide phase even in the specimen with 15 at % C, i.e., in the specimen where solidification started from the eutectic decomposition of liquid rather than from the formation of primary carbide crystals. Thus, the formation of the NbC phase is most likely to be related to the peculiarities of the Nb–Mo–C diagram in the composition region under study. As follows from the experimental data, the formation of binary M–MC eutectics is characteristic of this composition region. The volume fractions of carbides additionally support this hypothesis. Clearly, if an M_2C-based carbide with about 33 at % carbon formed in a sample with 30 at % carbon, the volume fraction of the formed carbide would be about 90 vol %. However, the experimentally determined volume fraction of carbide the alloy was <70 vol %. Moreover, the obtained experimental data on the volume fractions of the phases enable us to eval-

Table 2. Experimental and calculated volume fractions of carbide phase in alloy specimens with various carbon contents

Characteristic	Value of characteristic for alloy specimens			
	15 at % C	20 at % C	25 at % C	30 at % C
Fraction of primary carbides, vol %	0	21	38	60
Total carbide fraction, vol %: experiment	~25	42	49	67
calculation for 42 at % C in NbC	29	40	52	65
calculation for 43 at % C in NbC	28	39	50	63

uate the carbon content in the MC carbide formed in the alloys. The fractions of phases in the alloys with 15, 20, 25, and 30 at % calculated by the lever rule give the best coincidence with the experimental data when the calculations were carried out at a carbon content of 42–43 at % in the carbide (Table 2). It should be noted that cubic NbC-based carbides are characterized by a wide homogeneity range in carbon content and the lower boundary of their regions in carbon content is a level of about 42 at %.

The lever rule for these calculations was used along the line of the equiatomic metal content in the ternary Nb–Mo–C diagram. In spite of the fact that this line is not a conode, the lever ratio along this line corresponds to the lever ratio also along the true conodes due to the similarity of the triangles formed by the conode, the constant carbon content lines, and the equiatomic metal content line on which the alloy compositions lie.

Thus, the XRD data of the existence of an MC-based carbide agree well with the results of studying the microstructure.

Mechanical Properties of the Alloys

Changes in the structural state of the alloys influence both their low- and high-temperature mechanical properties. A decrease in the short-time strength when the carbon content increases and, correspondingly, the fraction of metallic phase decreases deteriorate the capability of the latter to stress relaxation due to dislocations accumulated at carbide boundaries, making the alloys more brittle. The alloy specimens with 15 at % C have the maximum short-time strength at room temperature and at 1500°C (Fig. 4), namely, 400 and 1050 MPa, respectively. When the carbon content increased, these values smoothly decreased to 280 and 780 MPa, respectively, in the alloy with 30 at % C. The relatively low short-time strengths are likely be related to the existence of coarse primary (Nb,Mo)C carbide precipitates.

The dependence of the creep rate on the stress and temperature of the alloys is well described in this temperature range by the expression $\dot{\varepsilon} = k\sigma^n \exp Q/(kT)$, which is characteristic of dislocation creep (Q is the activation energy). As was shown earlier for eutectic Nb–Si alloys, the creep rate at exponent n close to 1 is determined by the rate of active dislocation climb along the matrix–solid particle interface in a matrix phase. At $n > 1$, conservative dislocation motion in a hardening phase contributes to the total strain [3]. As is seen from the data in Fig. 5, n is in the range 0.82–2.25 for all alloys. This fact implies that dislocations in carbide particles contribute to the total strain of a specimen at 1500°C.

The alloy specimens with 15 at % C also demonstrate the best high-temperature properties. The 100-h creep strength has record-breaking values: σ_{100}^{1500} (intersection point of creep line and horizontal line in a plot) is 210–300 MPa.

CONCLUSIONS

(1) The elemental, phase, and structural state of a series of Nb–Mo–C alloys with an equiatomic metal content and 15, 20, 25, and 30 at % C were studied. The structure of the alloys consists of a molybdenum-based solid solution matrix and a reinforcing niobium carbide–based solid solution. The structural state of all alloys corresponds to the binary eutectic in the ternary Nb–Mo–C system; here, an alloy with 15 at % is eutectic and alloys containing 20 at % or more are hypereutectic.

(2) The main phases in all alloys are a molybdenum-based bcc solid solution and an NbC-based

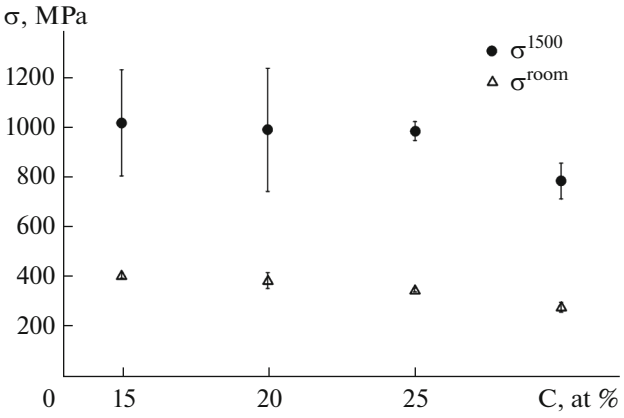

Fig. 4. Short-time strength of alloys with various carbon contents at room temperature and at 1500°C.

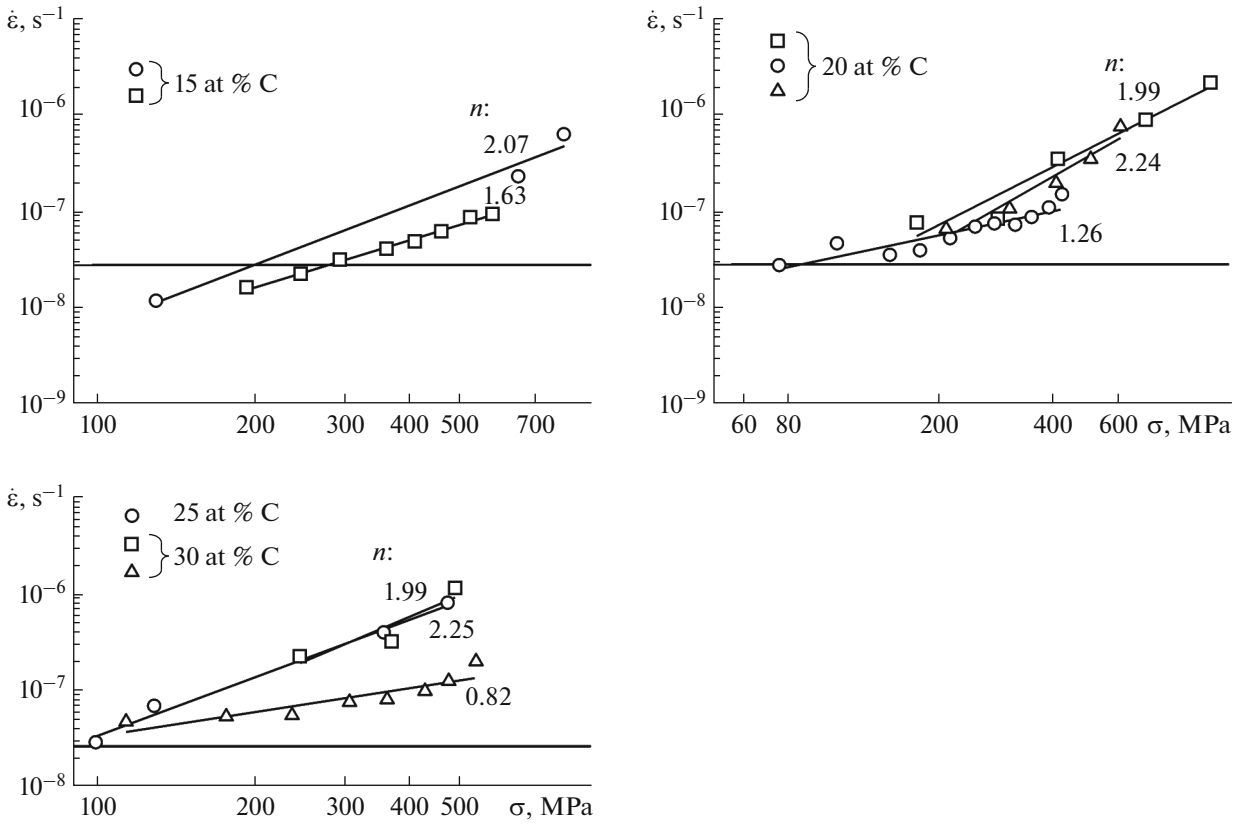

Fig. 5. Creep strain rate $\dot{\varepsilon}$ of alloys with various carbon contents vs. stress σ at 1500°C.

cubic carbide. The formation of cubic carbide stable and reproducible in all specimens is most likely to reflect the corresponding configuration of the phase diagram in the alloy composition region under study. The hypotheses about the relation of the carbide stoichiometry with the nucleation of primary crystals and their metastability seem to be a less probable explanation of the observed phenomena.

(3) The molybdenum content in both phases increases with the carbon content in an alloy. EPMA data agree with XRD data, which also demonstrate an increase in the molybdenum content in both phases with the average carbon content in the alloy.

(4) When the temperature increases from room temperature to 1500°C, the short-time strength of all alloys increases by a factor of 2.5–3 and reaches about 1000 MPa at 1500°C. This fact indicates a high potential of the high-temperature strength and also an insufficient toughness of the metallic matrix at room temperature.

(5) Creep tests demonstrated a low reproducibility of results, which makes it impossible to compare alloys with each other reliably. Nevertheless, the data obtained in this work allow us to estimate the level of 100-h strength at 1500°C for the alloys at 200–300 MPa in spite of the significant increase in the ductility of the matrix at high temperatures. This is very high value, which demonstrates the prospects of using Nb–Mo–C alloys as high-temperature materials.

FUNDING

This work was supported by the Russian Foundation for Basic Research, project no. 19-02-00434.

CONFLICT OF INTEREST

The authors declare that they have no conflicts of interest.

REFERENCES

1. S. J. Balsone, B. P. Bewlay, M. R. Jackson, P. R. Subramanian, J. C. Zhao, A. Chatterjee, and T. M. Heffernan, "Materials beyond superalloy-exploiting high-temperature composites," in *Structural Intermetallics* (Miner., Metals Mater. Soc. AIME, 2001), pp. 99–108.
2. T. M. Pollock, "Alloy design for aircraft engines," Nat. Mater. **15** (8), 809–815 (2016).
3. I. L. Svetlov, M. I. Karpov, T. S. Stroganova, D. V. Zaitsev, and Yu. Artemenko, "High-temperature creep in situ Nb–Si composites," Deform. Razrushenie Mater., No. 11, 2–6 (2019).
4. I. L. Svetlov, M. I. Karpov, A. V. Neuman, and T. S. Stroganova, "Temperature dependence of the ultimate strength of in situ multicomponent Mb–Si–X

(X = Ti, Hf, W, Cr, Al, and Mo) composites," Deform. Razrushenie Mater., No. 10, 17–22 (2017).

5. S. Miura, M. Aoki, Y. Saeki, K. Ohkubo, T. Mohri, and Y. Mishima, "Effects of Zr on the eutectoid decomposition behavior of Nb_3Si into (Nb)/Nb_5Si_3," Met. Mater. Trans. A **36** (3), 489–496 (2005).
6. K. Chattopadhyay, R. Sinha, R. Mitra, and K. K. Ray, "Effect of Mo and Si on morphology and volume fraction of eutectic in Nb–Si–Mo alloys," Mater. Sci. Eng. A **456** (1–2), 358–363 (2007).
7. K. S. Chan and D. L. Davidson, "Improving the fracture toughness of constituent phases and Nb-based in situ composites by a computational alloy design approach," Met. Mater. Trans. A **34** (9), 1833–1849 (2003).
8. J. Sha, H. Hirai, T. Tabaru, A. Kitahara, H. Ueno, and S. Hanada, "High-temperature strength and room-temperature toughness of Nb–W–Si–B alloys prepared by arc melting," Mater. Sci. Eng. A **364** (1–2), 151–158 (2004).
9. C. L. Ma, J. G. Li, Y. Tan, R. Tanaka, and S. Hanada, "Microstructure and mechanical properties of Nb/Nb_5Si_3 in situ composites in Nb–Mo–Si and Nb–W–Si systems," Mater. Sci. Eng. A **386** (1–2), 375–383 (2004).
10. Q. Wang, C. Zhou, and S. Wang, "Effect of Zr and Hf additions on microstructure and mechanical properties of Nb–Si based ultrahigh-temperature alloys," J. Mater. Res. Technol. **9** (6), 15585–15592 (2020).
11. R. Ma and X. P. Guo, "Effects of V addition on the microstructure and properties of multielemental Nb–Si based ultrahigh-temperature alloys," J. Alloys Compd. **845**, 156254 (2020).
12. R. Ma and X. P. Guo, "Influence of molybdenum content on the microstructure, mechanical properties, and oxidation behavior of multi-elemental Nb–Si based ultrahigh-temperature alloys," Intermetallics **129**, 107053 (2021).
13. J. Geng and P. Tsakiropoulos, "A study of the microstructures and oxidation of Nb–Si–Cr–Al–Mo in situ composites alloyed with Ti, Hf, and Sn," Intermetallics **15** (3), 382–395 (2007).
14. R. Ding, I. P. Jones, and H. Jiao, "Effect of Mo and Hf on the mechanical properties and microstructure of Nb–Ti–C alloys," Mater. Sci. Eng. A **458** (1–2), 126–135 (2007).
15. R. Ding, H. Jiao, and I. P. Jones, "Effect of Mo on mechanical properties and microstructure of Nb–Ti–C alloys," Mater. Sci. Eng. A **483–484** (1–2), 199–202 (2008).
16. X. Zhang, X. He, C. Fan, Y. Li, G. Song, Y. Sun, and J. Huang, "Microstructural and mechanical characterization of multiphase Nb-based composites from Nb–Ti–C–B system," Intern. J. Refract. Metals Hard Mater. **41**, 185–190 (2013).
17. Y. Tan, C. L. Ma, A. Kasama, R. Tanaka, Y. Mishima, S. Hanada, and J. M. Jang, "Effect of alloy composition on microstructure and high-temperature properties of Nb–Zr–C ternary alloys," Mater. Sci. Eng. A **341** (1–2), 282–288 (2003).
18. Z. W. Shi, J. L. Liu, and H. Wei, "Investigation on the microstructure and mechanical behaviors of a laser formed Nb–Ti–Al alloy," Mater. Char. **162**, 110193 (2020).
19. W. Wei, J. Sun, S. Zhang, B. liu, K. Yan, J. Qi, and H. Zhang, "Phase precipitation behavior and mechanical properties of multiphase Nb–Ti–C and Nb–Ti–Al—C," Mater. Sci. Eng. A **815**, 141218 (2021).
20. Q. Wei, G. Luo, J. Zhang, S. Jiang, P. Chen, Q. Shen, and L. Zhang, "Designing high-entropy alloy–ceramic eutectic composites of $MoNbRe_{0.5}TaW(TiC)_x$ with high compressive strength," J. Alloys Compd. **818**, 152846 (2020).
21. S. Y. Kamata, D. Kanekon, Y. Lu, N. Sekido, K. Maruyama, G. Eggeler, and K. Yoshimi, "Ultra-high-temperature tensile creep of TiC-reinforced Mo–Si–B–based alloy," Sci. Rep. **8** (1), 1–14 (2018).
22. T. S. Stroganova, M. I. Karpov, V. P. Korzhov, V. I. Vnukov, D. V. Prokhorov, I. S. Zheltyakova, I. B. Gnesin, and I. L. Svetlov, "Influence of titanium and molybdenum on the structure and mechanical properties of in situ niobium–silicon-based composite," Izv. Ross. Akad. Nauk, Ser. Fiz. **79** (9), 1300–1304 (2015).
23. X. Zhang, Y. Li, X. He, X. Liu, Q. Jiang, and Y. Sun, "Microstructural characterization and mechanical properties of Nb–Ti–C–B in situ composites with W addition," Mater. Sci. Eng. A **646**, 332–340 (2015).
24. M. Fujikura, A. Kasama, R. Tanaka, and S. Hanada, "Effect of alloy chemistry on the high-temperature strength and room-temperature fracture toughness of advanced Nb-based alloys," Mater. Trans. **45** (2), 493–501 (2004).
25. I. L. Svetlov, O. G. Ospennikova, M. I. Karpov, and Yu. V. Artemenko, "High-temperature borosilicate molybdenum alloys strengthened by titanium carbides. Mo–Si–B–TiC (Review)," Materialovedenie, No. 9, 16–33 (2020).
26. M. I. Karpov, D. V. Prokhorov, V. I. Vnukov, T. S. Stroganova, B. A. Gnesin, I. B. Gnesin, I. S. Zheltyakova, and I. L. Svetlov, "Structure and high-temperature mechanical properties of high-carbon niobium-based alloys," Deform. Razrushenie Mater., No. 5, 12–18 (2019).
27. S. A. Saltykov, *Stereometric Metallography*, Metallurgiya, Moscow, 1976).
28. J. Schindelin, I. Arganda-Carreras, E. Frise, et al., "An open-source platform for biological-image analysis," Nature Methods **9** (7), 676–682 (2012).

Translated by Yu. Ryzhkov